FAST NEUTRON TOTAL AND SCATTERING CROSS SECTIONS OF CHROMIUM, IRON AND ^{60}Ni

by

A.B. Smith, P.T. Guenther and J.F. Whalen

Prepared for

NEANDC Topical Discussion

Central Bureau for Nuclear Measurement

Geel, Belgium

September 18, 1979

UofC-AUA-USDOE

ARGONNE NATIONAL LABORATORY, ARGONNE, ILLINOIS

Operated under Contract W-31-109-Eng-38 for the

U. S. DEPARTMENT OF ENERGY

FAST-NEUTRON TOTAL AND SCATTERING CROSS SECTIONS OF CHROMIUM, IRON AND ^{60}Ni*

by

A. B. Smith, P. T. Guenther and J. F. Whalen

Applied Physics Division
Argonne National Laboratory
Argonne, Illinois, U.S.A.

ABSTRACT

Neutron total cross sections are measured with broad resolutions (50-100 keV) from ≈1.0 - 4.5 MeV at intervals of $\lesssim$50 keV and to accuracies of ≈1%. Differential elastic scattering cross sections are measured at $\geq$ 10 scattering angles distributed between 20-160 deg. from ≈1.5 - 4.0 MeV at intervals of $\lesssim$50 keV. Angle-integrated elastic scattering cross sections are deduced from the measured values to accuracies of $\gtrsim$5%. Inelastically scattered neutrons are observed up to incident neutron energies of 4.0 MeV at scattering angles distributed between 20-160 deg. Cross sections are determined corresponding to the excitation of "observed states" at; 1) Chromium; 1433, 2377, 2665, 2778 and 2970 keV, 2) Iron; 853, 1389, 2097, 2579, 2677, 2974 and 3152 keV, and 3) ^{60}Ni; 1342, 2168, 2304, 2509, 2636 and 3164 keV. The experimental results are discussed in terms of conventional optical-statistical models and in the context of direct-scattering processes. The experimental and calculational results are compared with the corresponding evaluated quantities given in the ENDF/B file.

Prepared for the topical discussion of the NEANDC, September 1979.

*This work performed under the auspices of the U.S. Department of Energy.

I. INTRODUCTION

In preparation for, at and subsequent to the NEANDC/NEACRP Specialist meeting on Nuclear Data of Structural Materials for Fast Reactors (1) it became clear that fast neutron data for the primary constituents of stainless steel were remarkably deficient. For example, much of the chromium ENDF-IV file appeared essentially a model construction. It was also evident that many of the data needs in this area (2) could be met with relatively modest application of existing measurement systems and techniques. These observations stimulated new interest in structural-material measurements at Argonne. This report outlines new results thus far obtained in this renewed effort.

The objective was the measurement of energy-averaged neutron total and scattering cross sections of chromium, iron and nickel so as to provide the neutron elastic and inelastic scattering cross sections to the requested accuracies of ≈5% over the energy range 1-5 MeV. The procedure was the measurement of broad-resolution neutron total and elastic scattering cross sections to accuracies that imply a non-elastic cross section to an uncertainty of ≈5%. Concurrently, neutron inelastic cross sections were sought consistent with the non-elastic cross section and to the same accuracies. This procedure implies energy-averaged total neutron cross section accuracies of ≈1% and neutron scattering cross sections to accuracies of ≈5%.

Generally, the detailed aspects of this work are given in the Laboratory reports of Refs. 3-6.

II. MEASUREMENT METHODS

A. Samples

All measurement samples were fabricated into cylinders from high-chemical-purity metal. The chromium and iron samples consisted of elemental material while the nickel sample was essentially 100% enriched in the isotope ^{60}Ni. All scattering samples were approximately 2 cm in diameter and 2 cm long. The chromium and iron total-cross-section samples varied in length so as to provide a number of transmissions over the range of 20-80%. The ^{60}Ni total cross sections were determined using the scattering sample with neutrons incident upon the cylinder base.

B. Neutron Total Cross Sections

The neutron-total-cross-section measurements were made using the monoenergetic-source facilities at the Argonne National Laboratory Fast Neutron Generator. The neutron source was the $^{7}Li(p;n)^{7}Be$ reaction produced by a proton burst of ≈1 nsec duration incident on a lithium metal film at a repetition rate of 2 MHz. The energy of the resulting neutrons was governed by the proton energy and the neutron-energy resolution was controlled

by the thickness of the lithium-target film. A shield and associated collimator around the source were used to obtain a neutron beam ≈1 cm in diameter at a zero-degree source-reaction angle. The samples were, including the carbon of and a void, placed upon a wheel so that they rotated through the beam at a repetition rate of approximately 20 cpm. In all cases the neutron beam was incident on the bases of the cylindrical samples. The neutron detector was a proton-recoil scintillator placed on the neutron-beam axis approximately 5 m from the neutron source. Conventional time-of-flight techniques were used to obtain the velocity spectra of neutrons arriving at the detector. The observed spectra were correlated with the sample (or void) positions using an on-line computer system. The prominent neutron peak observed in the velocity spectra corresponding to the primary yield of the source reaction was integrated to obtain the detector response rate. Backgrounds and source perturbations were small and easily determined from an analysis of the velocty spectra. A random signal was introduced into the data acquisition system in order to precisely determine dead-time corrections. In-scattering corrections were estimated and found to be negligible. The neutron transmissions through the samples followed directly from the observed detector responses. The total cross sections were calculated from the transmissions in the conventional manner (7). An ancillary experiment utilized the same apparatus to determine the neutron total cross sections of sulfur, silicon and carbon over selected energy intervals with resolutions of 2-5 keV. The results were correlated with well known resonance structure in these elements in order to determine the energy scale of the apparatus to within ≈10 keV; i.e. to values approximately an order of magnitude less than the resolutions employed in the present mdeasurements.

C. Neutron Scattering Measurements

The neutron scattering measurements were made using the Argonne National Laboratory 10-angle, pulsed-beam time-of-flight system using the above pulsed $^{7}Li(pn,n)^{7}Be$ source. The mean incident-neutron energy at the scattering sample was known to ≈10 keV. The scattering samples were placed ≈13 cm from the neutron source at a zero-degree reaction angle. Proton-recoil scintillators were placed at flight paths of 5 to 5.5 m. The flight paths were defined by a massive collimator system extending over a scattered-neutron angular range of 20 to 160 deg. The scattering angles were determined to a $\lesssim$0.5 deg. and an absolute accuracy of $\lesssim$1.0 deg. An independent time-of-flight system was used to monitor the source intensity, backed up by four "long counters." The relative energy dependencies of the scattered-neutron-detector sensitivities were determined by observation of neutrons scattered from hydrogen (polyethylene) at selected angles and a fixed incident energy or from measurements of the neutron spectrum emitted during the spontaneous fission of ^{252}Cf (8). The normalizations of the relative-detector sensitivities were determined by observing neutrons scattered from hydrogen (polyethylene) at selected energies and angles. Thus all scattering cross sections were determined relative to well known H(n,n) cross sections (9). The measured velocity spectra were reduced to cross sections and corrected for angular resolution, sample attenuation and multiple-event effects (8). Concurrent determinations of the elastic scattering cross sections of carbon verified the fidelity of the measurement system. In the case of ^{60}Ni there were some ancillary measurements of the (n;n',gamma) cross sections using conventional GeLi detector techniques (4).

III. EXPERIMENTAL RESULTS

A. Neutron Total Cross Sections

The objective of the total cross section measurements was the determination of precise energy-averaged magnitudes comparable with the subsequently measured scattering cross sections, model predictions and evaluations. Resolution of detailed resonance structure was explicitly avoided. The measured energy range varied somewhat from sample to sample but generally extended from 1.0 - 4.5 MeV with mesurements made at intervals of $\lesssim$50 keV with incident resolutions of >50 keV. The measurements with each particular sample were repeated several times with consistent results. In addition for the chromium and iron targets the measurements envolved at least four sample thicknesses extending over the range of ≈2-8 cm. The experimental values for a given sample thickness were averaged over incident energy intervals of 100 - 200 keV to obtain average values with a statistical accuracy of ≈1%. The energy-averaged results were appreciably dependent upon sample thickness as illustrated in Fig. 1. The results obtained with the thicker samples were very much lower than those obtained with the thin samples due to the appreciable self shielding of the samples. The results obtained with the various sample thicknesses were extrapolated to the zero-thickness value to obtain the "true" energy-averaged cross sections. In the case of iron very carefully measured and very high resolution results have been obtained by Harvey et al. (10). In this unusual case the resolution is sufficient to resolve the structure well into the MeV range and thus the average of the high resolution results should be consistent with the present broad-resolution values. The agreement is generally ≈1% as illustrated in Fig. 2. On the average, both of the measured sets of values tend to be systematically larger than a corresponding average constructed from the ENDF/B-IV file. The same general trend was observed in the comparison of the measured and evaluated neutron total cross sections of chromium shown in Fig. 3. These comparisons suggest that experimenters have not generally given proper consideration to the interplay of resolution, sample thickness and resonance structure and that, as a consequence, the neutron total cross section data base in the highly fluctuating structural region may be systematically distorted to too low values in the MeV range with consequent impact upon the evaluated files. Similar problems are known to occur in other mass-energy regions.

The ^{60}Ni neutron total cross section measurements had to be confined to a single and relatively thick sample. As a consequence the measured values are systematically lower than an equivalent average constructed from the better resolution results of Clement et al. (11) at lower energies as illustrated in Fig. 4. Numerical estimates suggest that the present values are distorted by 5-10% (or in the extreme 20%) toward too low values at energies below 1 MeV. This distortion rapidly decreases as the energy increases. There is no comparable ENDF/B file, but optical models based upon high-energy scattering measurements generally predict higher neutron total cross sections in this mass region and near 1 MeV. The discrepancies may be due in part to shortcomings in the models or physical behavior such as fluctuations, "doorways" (12), etc., that are not consistent with the underlying precepts of the optical model. However, the model-measurement discrepancy has

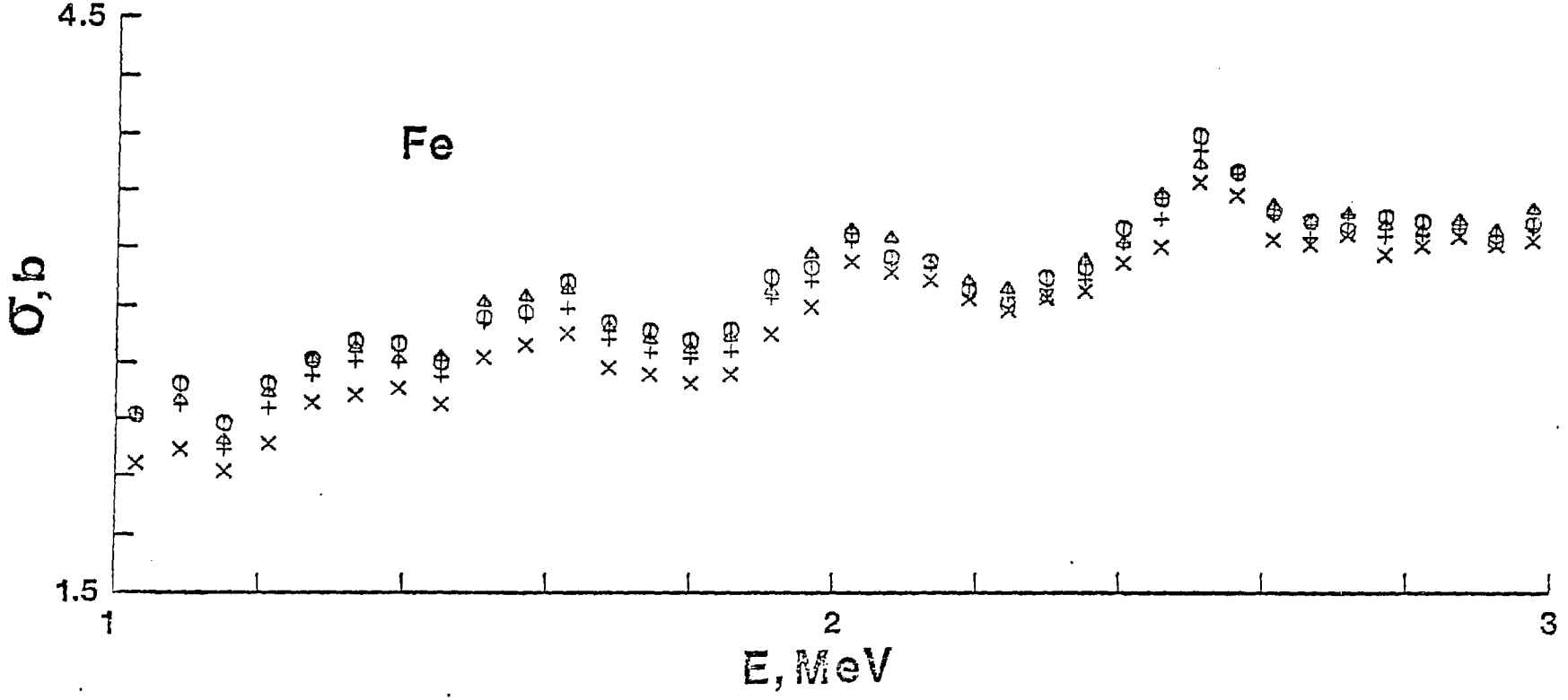

Fig. 1. Iron total neutron cross sections obtained with ≈200 keV resolution and 2(0), 2.5(Δ), 4(÷), and 8(X) cm thick samples.

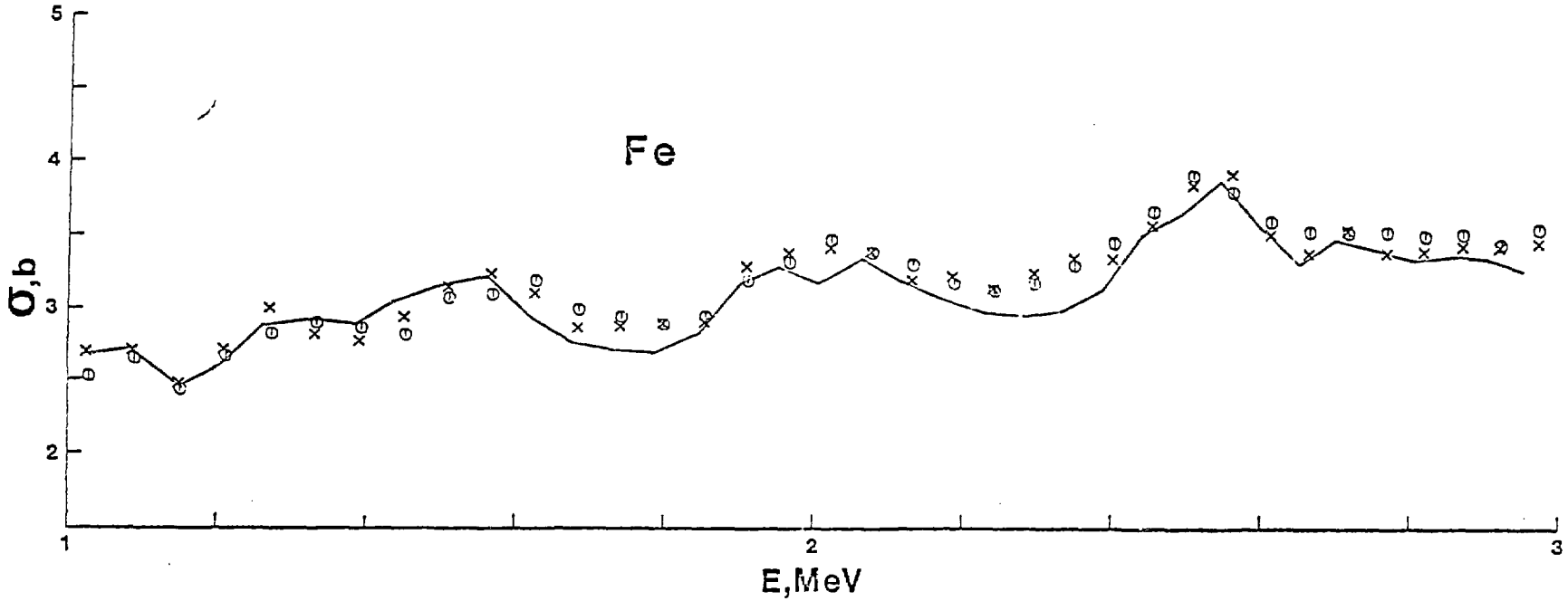

Fig. 2. Total neutron cross sections of iron. The present broad resolution measured values are indicated by data points (0). Equivalent average values constructed from the measured values of Harvey et al. (10) are indicated by data points (X). The respective average of ENDF/B-IV is indicated by the solid curve.

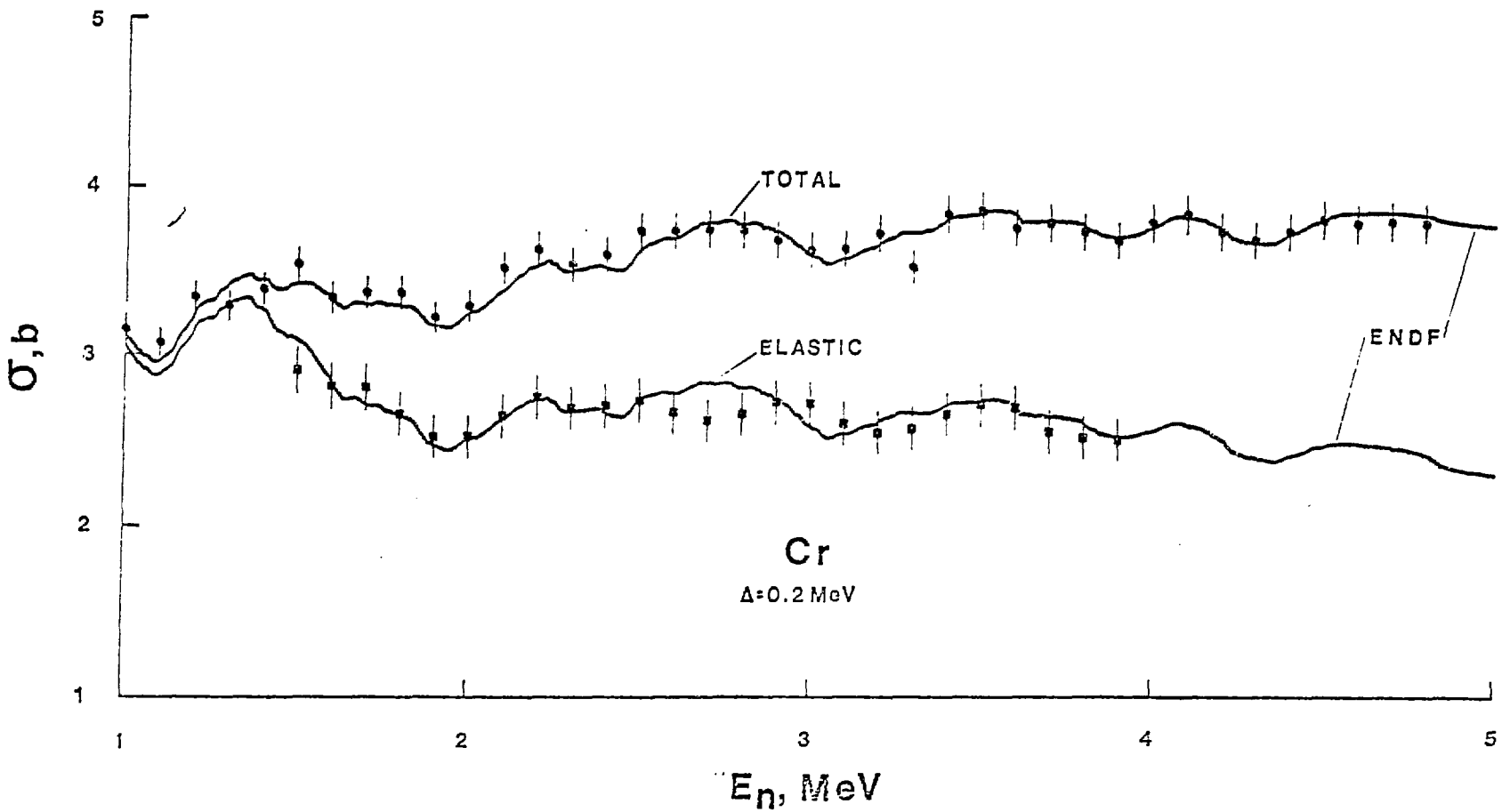

Fig. 3. Measured neutron total (0) and elastic (□) cross sections of elemental chromium averaged over incident-energy intervals of 200 keV compared with the equivalent averages constructed from the ENDF/B-IV file.

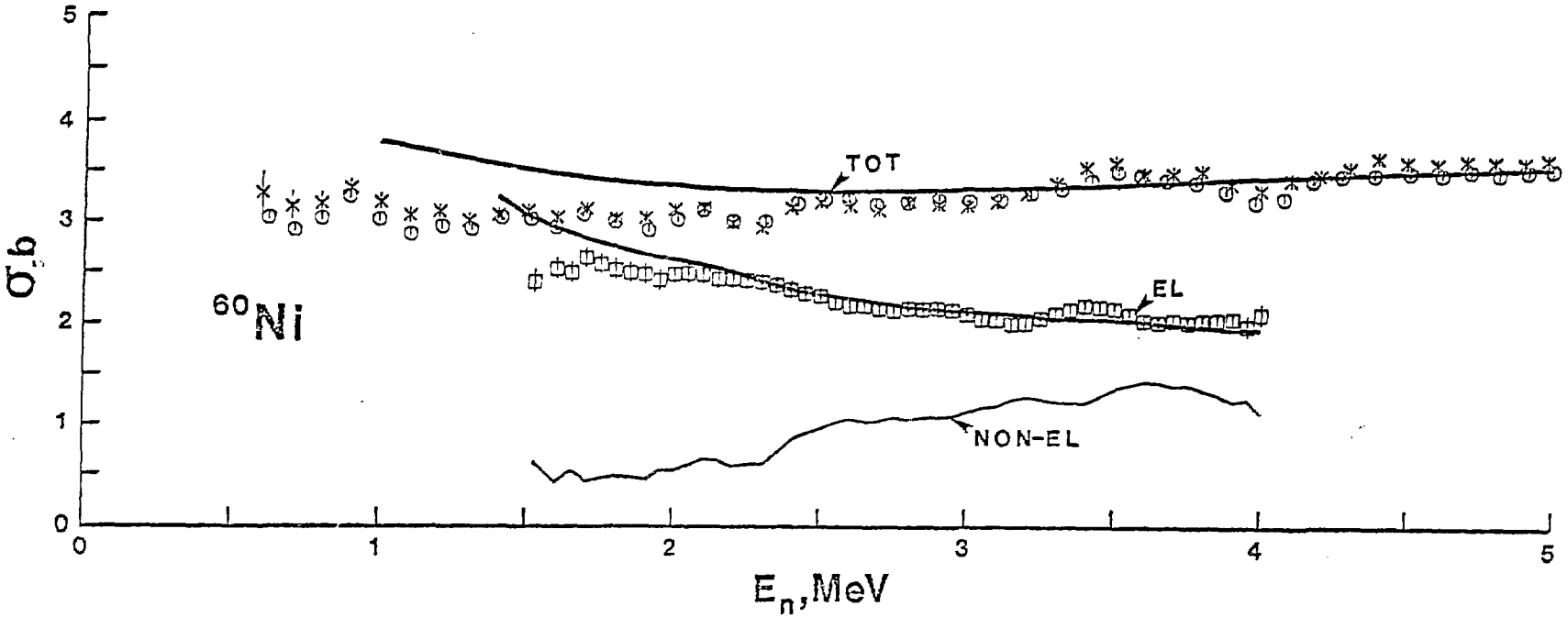

Fig. 4. Neutron Total and Elastic-Scattering Cross Sections of ^{60}Ni. 200 keV averages of the present results are indicated by (O) and (□) symbols, respectively. Comparable averages of the neutron total cross sections of Ref. 11 are noted by crosses. Curves indicate the results of model calculations and the non-elastic scattering cross section deduced from the present measurements.

been widely observed and an extreme example is shown in Fig. 4. Such discrepancies tend to be consistent with shortcomings in the experimental determinations of energy-averaged neutron total cross sections in this mass-energy region.

B. Neutron Elastic Scattering

Elastic neutron scattering cross sections were measured at incident energy intervals of ≤50 keV from 1.5 to 4.0 MeV with incident-energy resolutions of ≈20-60 keV. Measurements were made at ten or more scattering angles, distributed between 20 to 160 deg. for each incident energy. The objective was an angle-energy scope that would well define the elastic scattering cross sections to an intermediate energy resolution. The measurements were made at randomly selected energies or systematically over a predetermined energy range during various measurement periods. The individual differential scattering cross sections were generally determined to 5 to 8% accuracies. Statistical uncertainties contributed 1-3% to the overall uncertainties. Correction procedures, including those for effects due to angular uncertainties, made a similar small contribution. The largest contribution to the overall uncertainty came from the calibration of the detector efficiency (typically 3 to 5%). The uncertainty in the H(n,n) standard was a small factor (i.e. $\lesssim$1%).

Representative experimental results are outlined in Fig. 5. Despite the relatively-broad incident-energy resolutions, considerable variation in the distributions with energy is discernable throughout the measured energy range. Any single distribution is not necessarily representative of the more general energy-averaged behavior. A better representation of the average behavior is obtained by averaging the measured values over 200-keV intervals with results as illustrated in Figs. 6, 7 and 8. With these 200-keV averages, the behavior of the distributions varies reasonably smoothly with energy, and is comparable with predicitons of the energy-averaged models.

The 200-keV averages of the present results were least-square fitted with a Legendre polynomial expansion from which the angle-integrated elastic-scattering cross sections were derived. The accuracies of the latter were generally 3-5%, i.e. essentially dominated by the uncertainties associated with detector calibrations. Representative elastic-scattering cross sections are shown in Fig. 4. The angle-integrated elastic scattering cross sections fluctuate with energy in a manner consistent with the fluctuations of the neutron total cross sections. Together the two sets of cross sections yield the non-elastic cross sections. The non-elastic cross sections were generally consistent with the directly-measured neutron inelastic scattering cross sections above 1.5-2.0 MeV. On the average they were known to ≈5%.

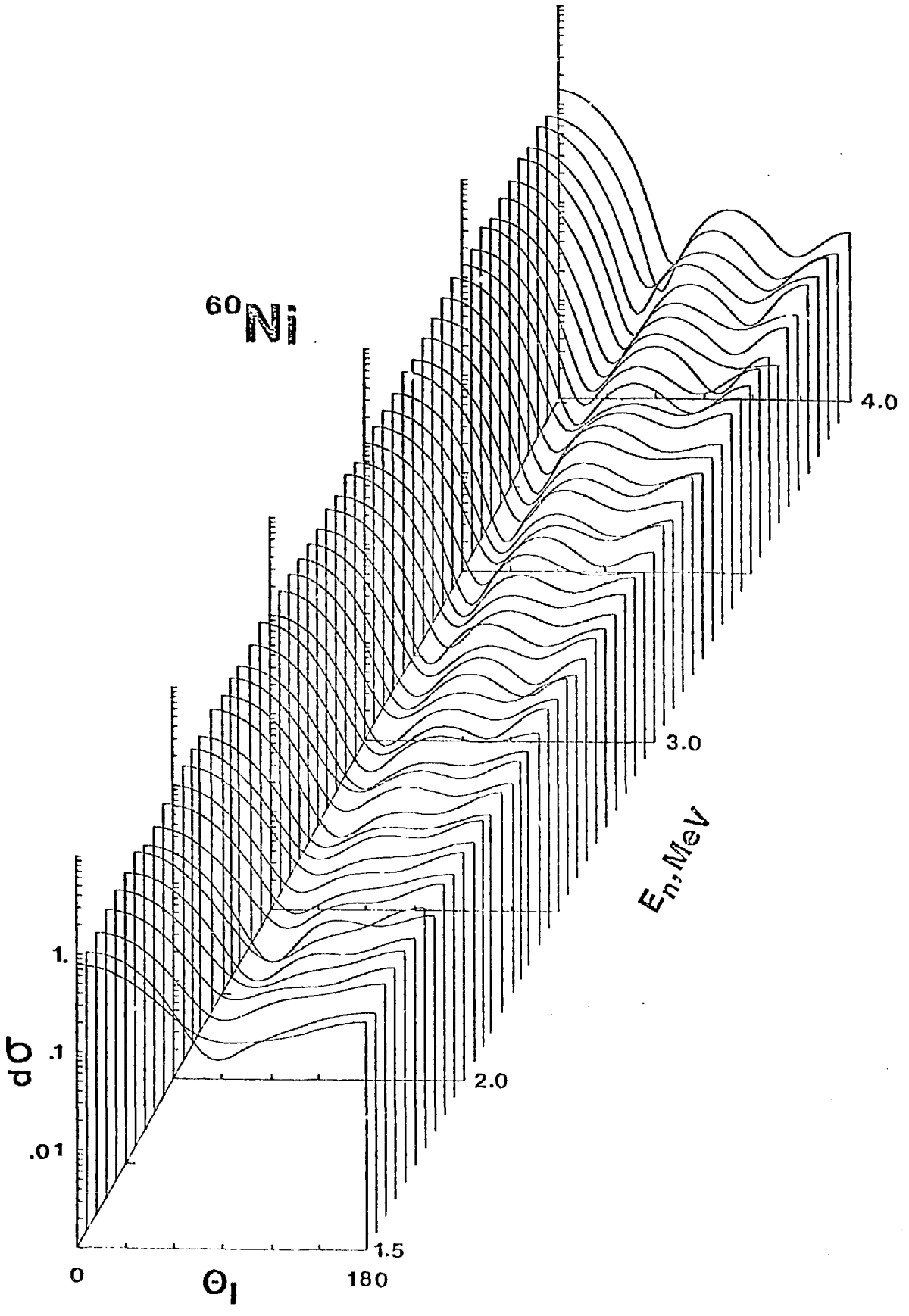

Fig. 5. Illustrative Differential Elastic-Neutron Scattering Cross Sections of ^{60}Ni. Incident-energy resolutions are 20-40 keV. Curves are the results of least-square fitting of Legendre-polynomial expansions to the actual measured values. Fluctuations with energy are evident

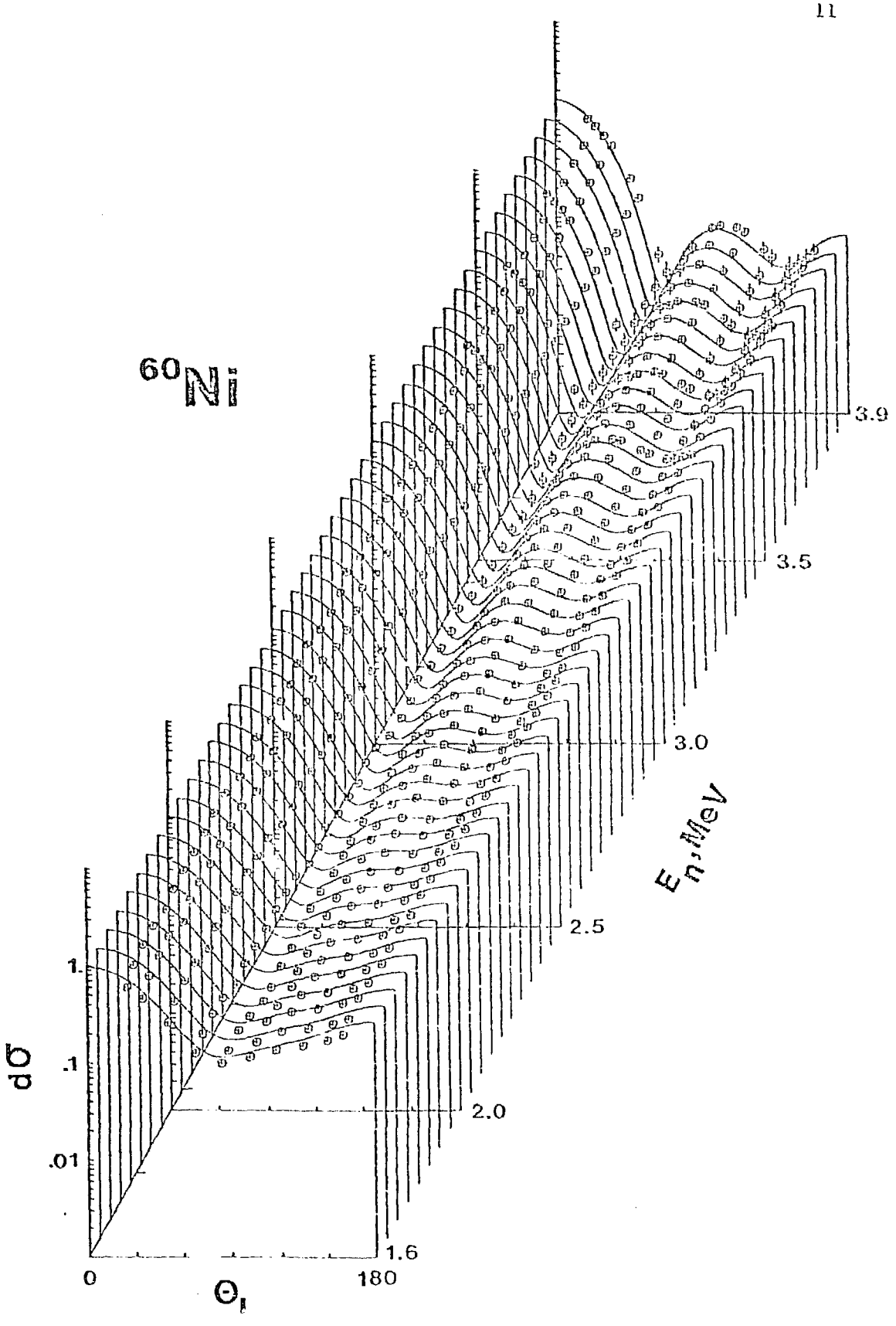

Fig. 6. Comparison of Measured (Data Points) and Calculated (Curves) Differential Elastic-Scattering Cross Sections of ^{60}Ni. (Cross sections are given as b/sr and angles as degrees in the lab system.)

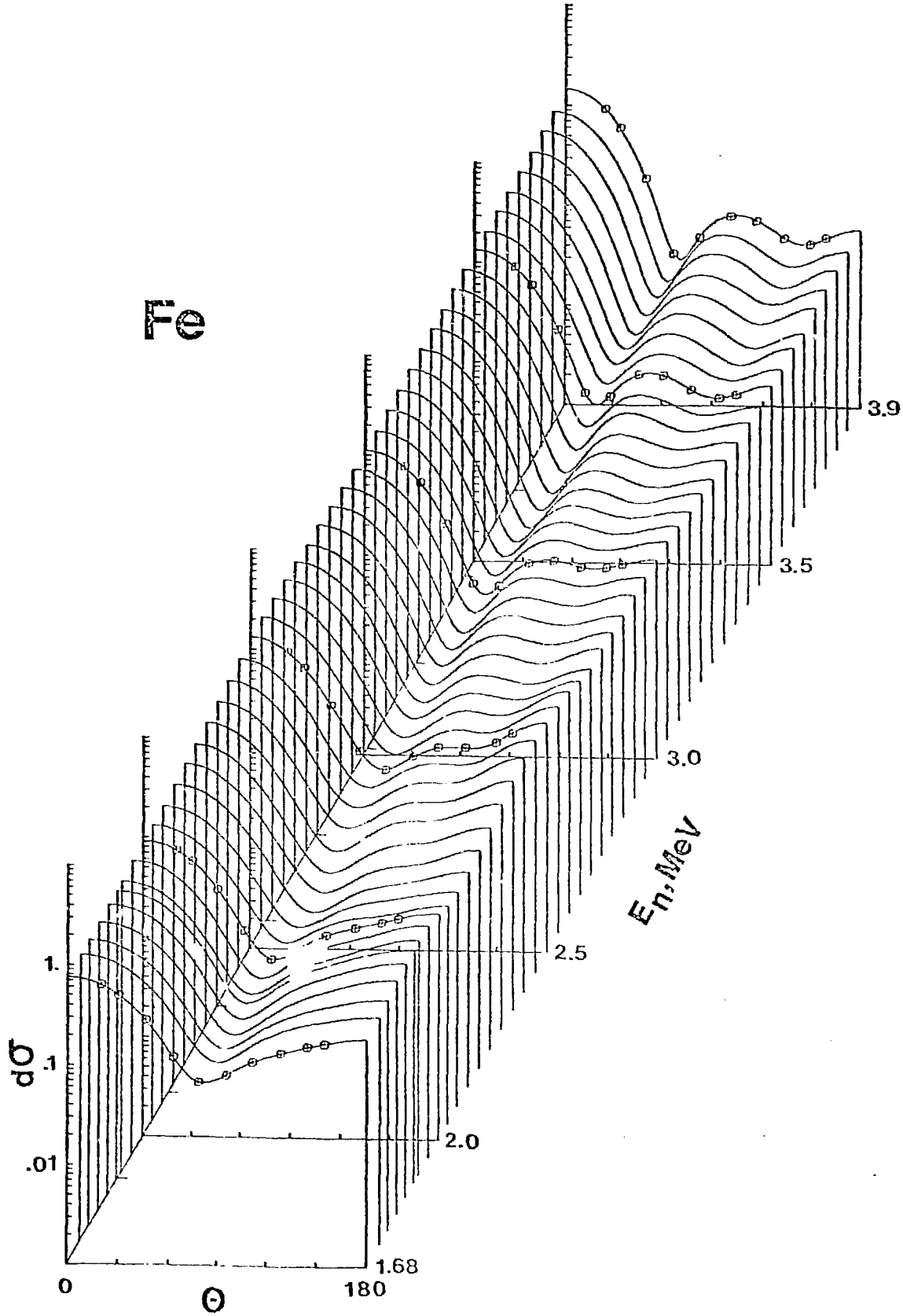

Fig. 7. The Present Measured Differential-Elastic-Scattering Cross Sections of Elemental Iron Averaged Over Incident-Energy Intervals of 200 keV. The curves are the result of least-squares fitting to Legendre-polynomial expansions.

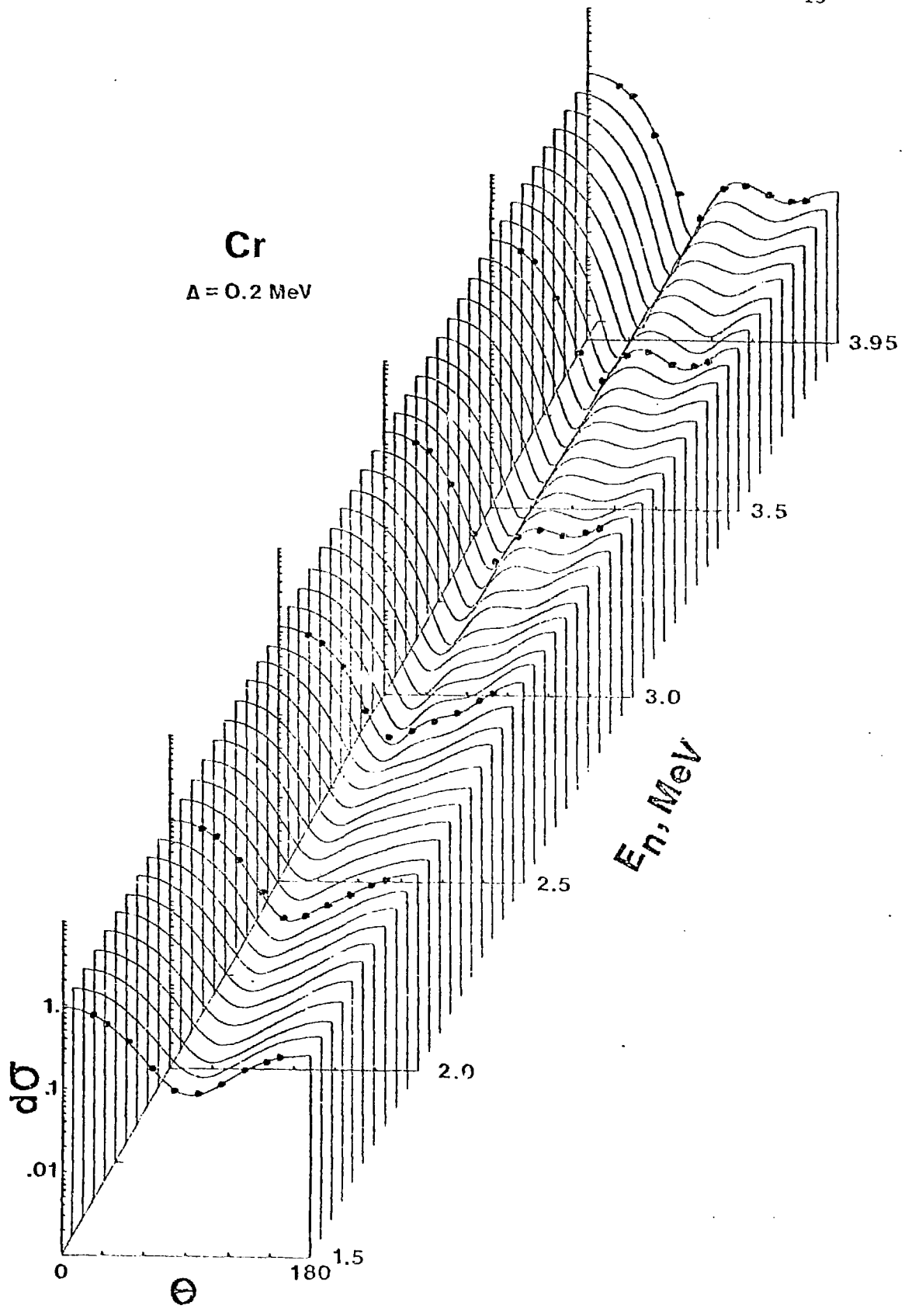

Fig. 8. The Present Measured Differential-Elstic-Scattering Cross Sections of Elemental Cr Averaged Over Incident-Energy Intervals of 200 keV. The notation is identical to that of Fig. 7.

C. Neutron Inelastic Scattering

Differential-neutron-inelastic-scattering cross sections were determined concurrently with the elastic-scattering values. Scattered neutrons were observed corresponding to levels in ^{60}Ni, chromium and iron as defined in Tables I, II and III. The excitation energies were determined from the measured incident energies, flight times and flight paths and were verified by the observation of well known inelastic-neutron groups (e.g. that due to excitation of the 846 keV level in ^{56}Fe). The above measured excitation energies are averages of a number of independent measurements and the uncertaintainties are RMS deviations from the mean. The presently-observed levels correspond reasonably well to known states in ^{60}Ni, chromium and iron as shown by the comparisons of Tables I, II and III. The correspondence is particualrly good to an excitation energy of ≃3.0 MeV.

Angle-integrated neutron inelastic-excitation cross sections were determined by least-square fitting no fewer than four differential values at each energy with Legendre polynomial series. The uncertainties in the differential-cross section values ranged from a minimum of ≈5% for prominent and well-resolved neutron groups at favorable energies to $\gtrsim$20% for less well resolved and/or low-intensity neutron groups. There was a similar spread in the uncertainties of angle-integrated cross sections ranging upward from a minimum of ≈5%. In addition to the complexities of experimental resolution and lesser experimental intensities, the inelastic-scattering uncertainties were subject to the same sources of uncertainty noted above in the elastic-scattering context.

A major feature of the inelastic process is the prominent excitation of the first, 2+, level. These levels are either vibrational (as in ^{60}Ni (13)) or rotational (as in ^{56}Fe (14)). The differential cross sections for the excitation of these levels fluctuate with energy in a manner analogous to that illustrated for the elastic scattering cross sections in Fig. 5. In order to remove these fluctuations the measured inelastic scattering distributions were averaged over ≈200 keV incident-neutron energy intervals in the same manner as for the elastic-scattering distributions. The resulting averages behaved in a relatively smooth manner as illustrated by the distributions for the 0.853 MeV state of ^{56}Fe shown in Fig. 9. Furthermore, this figure qualitatively shows the trend from distributions symmetric about 90 deg. at lower energies to those that are somewhat peaked forward at upper energies in a manner that could be expected as the result of increasing contributions from direct-inelastic processes. Cross sections for the excitation of higher-lying levels also fluctuated, and averaging procedures were used to obtain the energy-averaged behavior in the same fashion as outlined above for the first, 2+, levels. Scattered neutron distributions resulting from the excitation of these higher-lying levels were generally essentially symmetric about 90 deg.

Table I. Comparison of Observed and Reported Levels in ^{60}Ni

No.	E_x(MeV), Observed	E_x(MeV), Ref. 13
1	1.342 ± 0.013	1.333 (2+)
2	2.168 ± 0.010	2.158 (2+)
3	2.304 ± 0.026	2.296 (0+)
4	2.509 ± 0.022	2.506 (4+)
5	2.636 ± 0.019	2.625 (3+)
6	3.164 ± 0.041	3.123 (2+)
		3.184 (?)
		3.195 (1+)

Table II. Observed Inelastic-Neutron Excitations in Elemental Chromium

No.	E_x(MeV)	E_x(MeV)[a]	Isotopic Identification[a]
1	1.433 ± 0.009	1.434	Cr-52 (2+)
2	2.377 ± 0.008	2.321	Cr-53 (3/2-)
		2.370	Cr-52 (4+)
		2.455	Cr-53
3	2.665 ± 0.005	2.619	Cr-54 (2+)
		2.647	Cr-52 (0+)
		2.661	Cr-53 (5/2-)
		2.670	Cr-53
		2.711	Cr-53
4	2.778 ± 0.007	2.768	Cr-52 (4+)
		2.775	Cr-53
		2.826	Cr-53
		2.829	Cr-54 (0+)
5	2.970 ± 0.006	2.922	Cr-50 (2)
		2.965	Cr-52 (2+)
		2.995	Cr-53

[a] Taken from Ref. 13.

Table III. Observed Inelastic-Neutron Excitations in Elemental Iron

No.	E_x(MeV)	E_x(MeV)[a]	Isotopic Identification[a]
1	.853 ± 0.050	0.847	Fe-56 (2+)
2	1.389 ± 0.030	1.407	Fe-54 (2+)
3	2.097 ± 0.022	2.085	Fe-56 (4+)
4	2.579 ± 0.035	2.539	Fe-54 (4+) Fe-54 (0+)
5	2.677 ± 0.014	2.658	Fe-56 (2+)
6	2.974 ± 0.011	2.940 2.960 2.948 2.981	Fe-56 (0+) Fe-56 (2+) Fe-54 (6+) Fe-54 (2+)
7	3.152 ± 0.021	3.120 3.123 3.163	Fe-56 Fe-56 Fe-54

[a] Taken from Ref. 13.

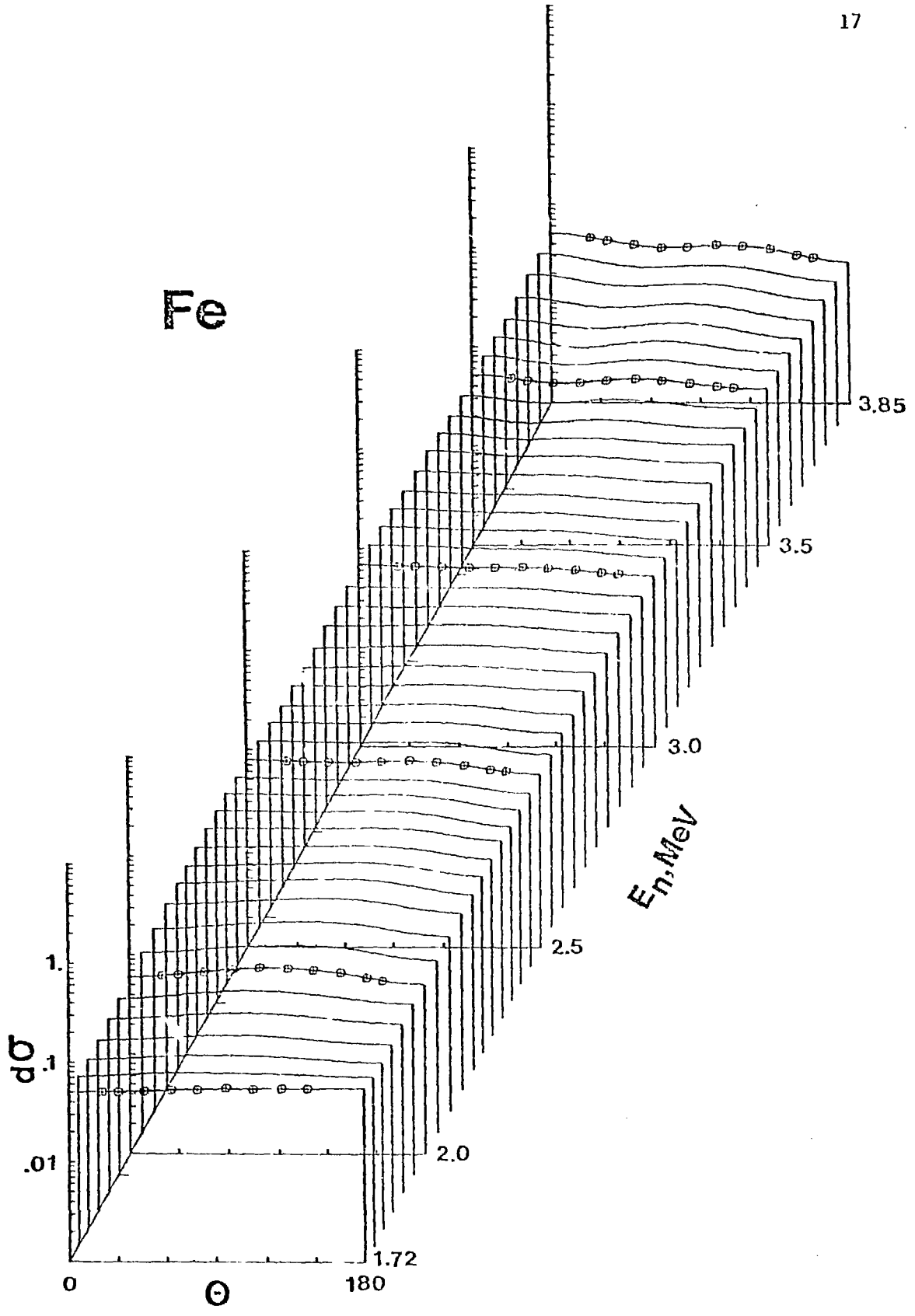

Fig. 9. Measured Differential Cross Sections for the Excitation of the 853 keV State in ^{56}Fe. The notation is identical to that of Fig. 7.

The above direct-neutron measurements extended to within ≈0.8 MeV of threshold. In the case of ^{60}Ni, (n,n',Y) techniques were used to extend the measured cross sections for the excitation of the prominent 1.342 MeV to threshold. The measured relative (n;n',Y)results were normalized to the directly measured (n;n') values near 2.0 MeV.

The angle-integrated neutron inelastic scattering cross sections derived from the direct neutron measurements are shown in Figs. 10, 11 and 12. There are a number of previously reported results some of which are indicated in these figures. The agreement with the present results varies from good to very poor. Many of these previous results consist of isolated or a few experimental values. The validity of comparisons of isolated values is questionable in view of the fluctuations in the cross sections and unavoidable variations in experimental energy scales and resolutions. Additional discussions of data comparisons are to be found in Refs. 3, 4 and 5.

Many of the present neutron-inelastic-scattering results can be compared with values given in the ENDF/B-IV files, corrected to isotopic quantities where necessary. The comparisons, indicated in Figs. 10, 11 and 12 suggest that those portions of the differential inelastic scattering files are discrepant with the present results by 15-20% or more. Some of these discrepancies appear in the largest inelastic excitation cross sections (e.g. the 2+ level of iron) and amount to 5-10% (or larger) discrepancies between measured and evaluated total neutron inelastic-scattering cross sections. The present inelastic-scattering results are further supported by their consistency with the above non-elastic cross sections to within ≈5%, i.e. to within the experimental uncertainties.

IV. INTERPRETATION

The experimental interpretations sought to: a) establish a spherical optical potential providing an acceptable description of the energy-averaged neutron cross sections in this mass-energy region of strong fluctuations, and 2) explore the effect of direct-inelastic processes in the neutron interaction. The scope and detail of the present experiments provides a suitable foundation for such investigations.

The spherical optical potential was entirely based upon the 200 keV averages of the measured differential elastic-scattering cross sections. The averaging increment was a compromise between a representation consistent with the concept of the optical model and the excited-level spacing influencing the compound-elastic component. The initial step in the deduction of the potential was a 6-parameter (real and imaginary strengths, radii and diffusenesses) Chi-square fit of a conventional surface-absorption optical potential to each of the measured elastic-scattering distributions. The compound-elastic contributions were calculated using the Hauser-Feshbach formula with width-fluctuation corrections (15, 16). The initial fitting procedures reasonably defined real and imaginary radii and diffusenesses. These four-parameters were then fixed for subsequent and more detailed two-parameter (real and imaginary strengths) Chi-square fitting procedures. The latter included the enhancement of compound-nucleus components using the formalism of Hofmann et al. (17). The level-density-distribution of Gilbert and Cameron (20) was used for the description of

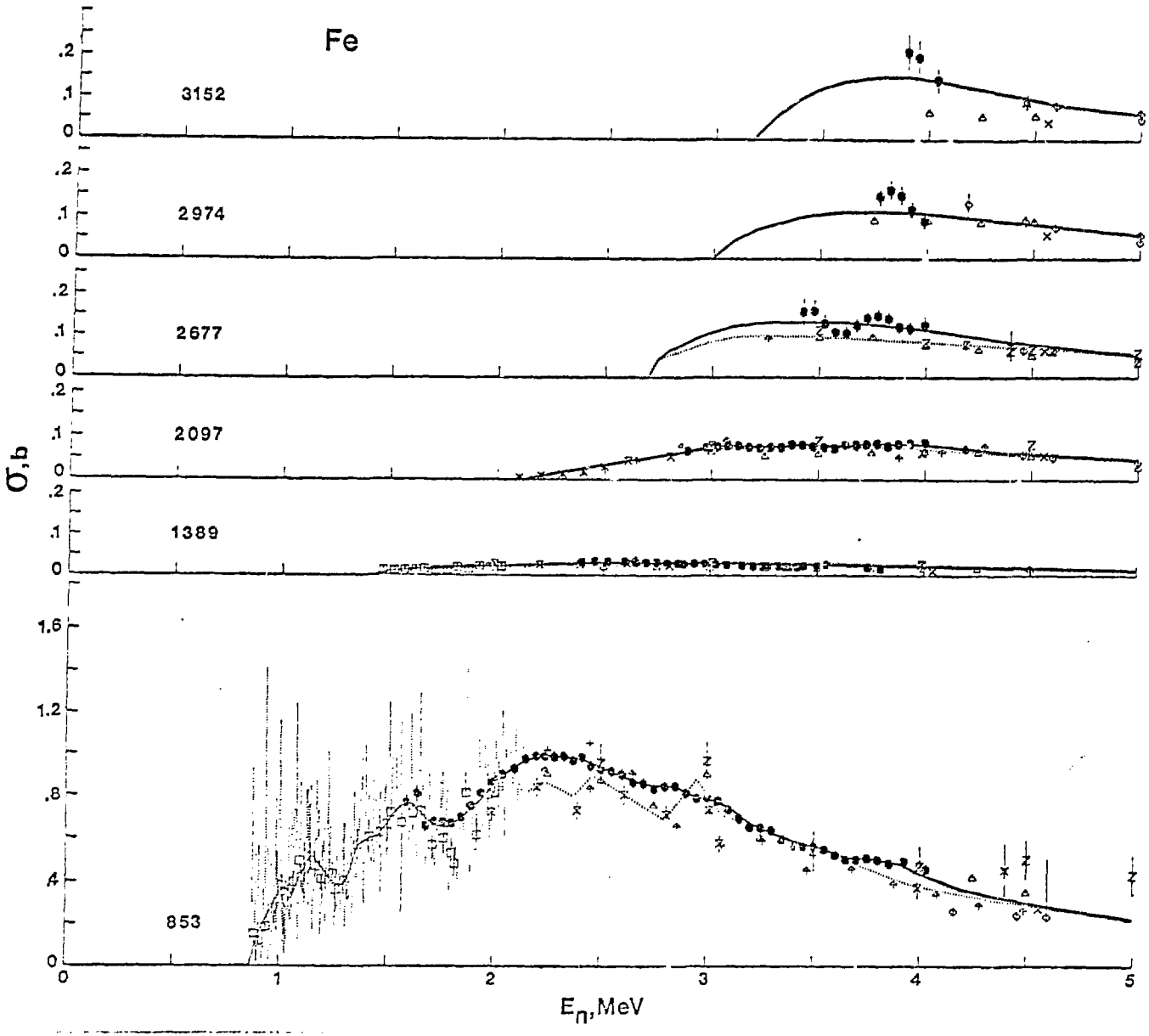

Fig. 10. Measured Inelastic Neutron Excitation Cross Sections of Elemental Iron. The present measured values are indicated by solid data symbols. Other symbols indicate experimental results as defined in Ref. 21. The solid curve is an "eye-guide" constructed through the present measurements. The dotted curve indicates the respective cross sections as given in ENDF/B-IV. Observed excitation energies are numerically given in keV for each section of the figure.

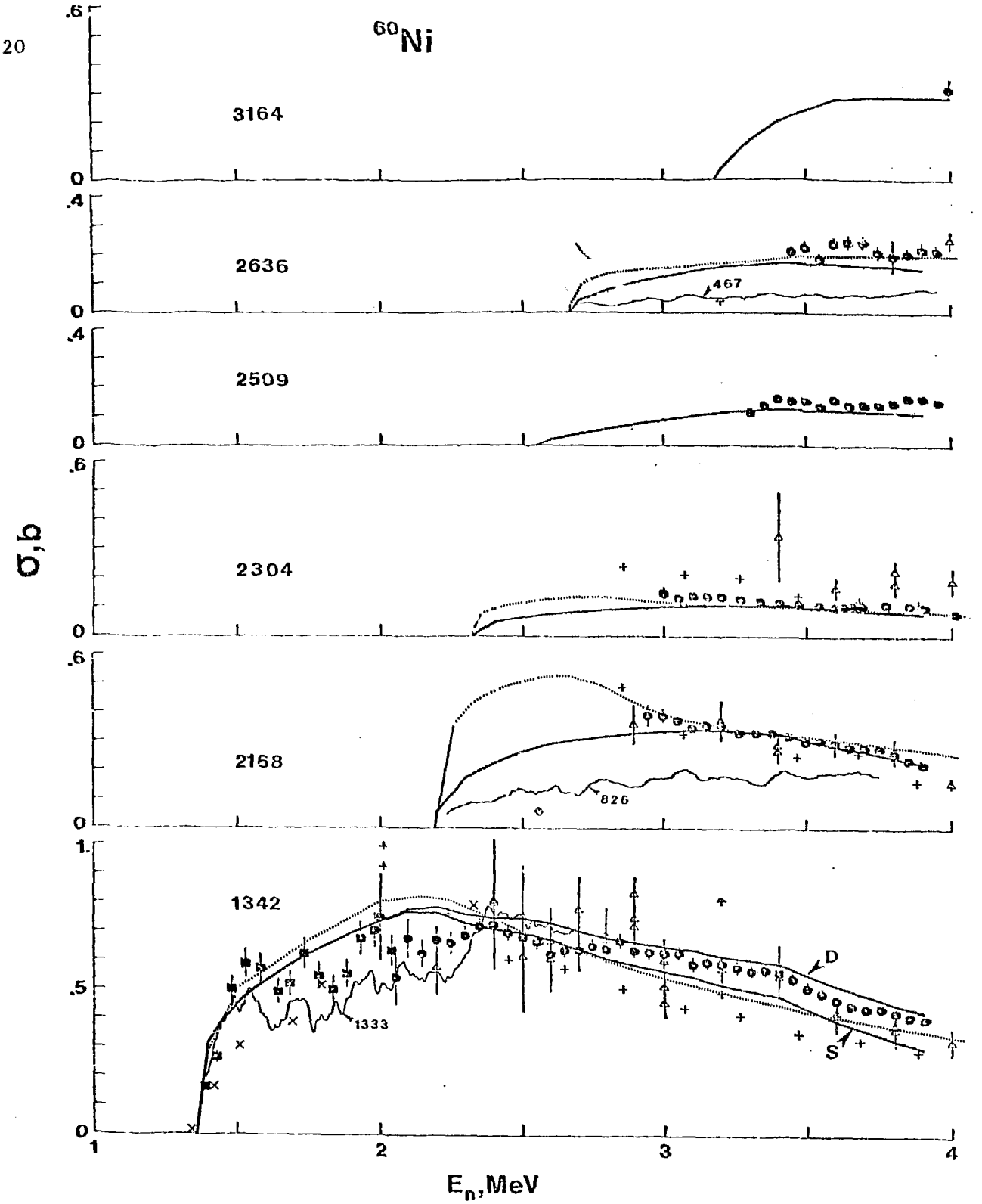

Fig. 11. Inelastic Neutron Excitation Cross Sections of ^{60}Ni. The present (n;n') results are noted by solid circular symbols, those from (n;n',γ) measurements by solid square symbols. Other symbols denote previously reported values as given in Ref. 4. Level excitation energies are numerically stated at the left of each section of the figure. Dashed curves indicate corresponding ENDF/B-IV values. Heavy solid curves denote results of model calculations as outlined in the text ("D" = result of deformed model, "S" or no notation = spherical model).

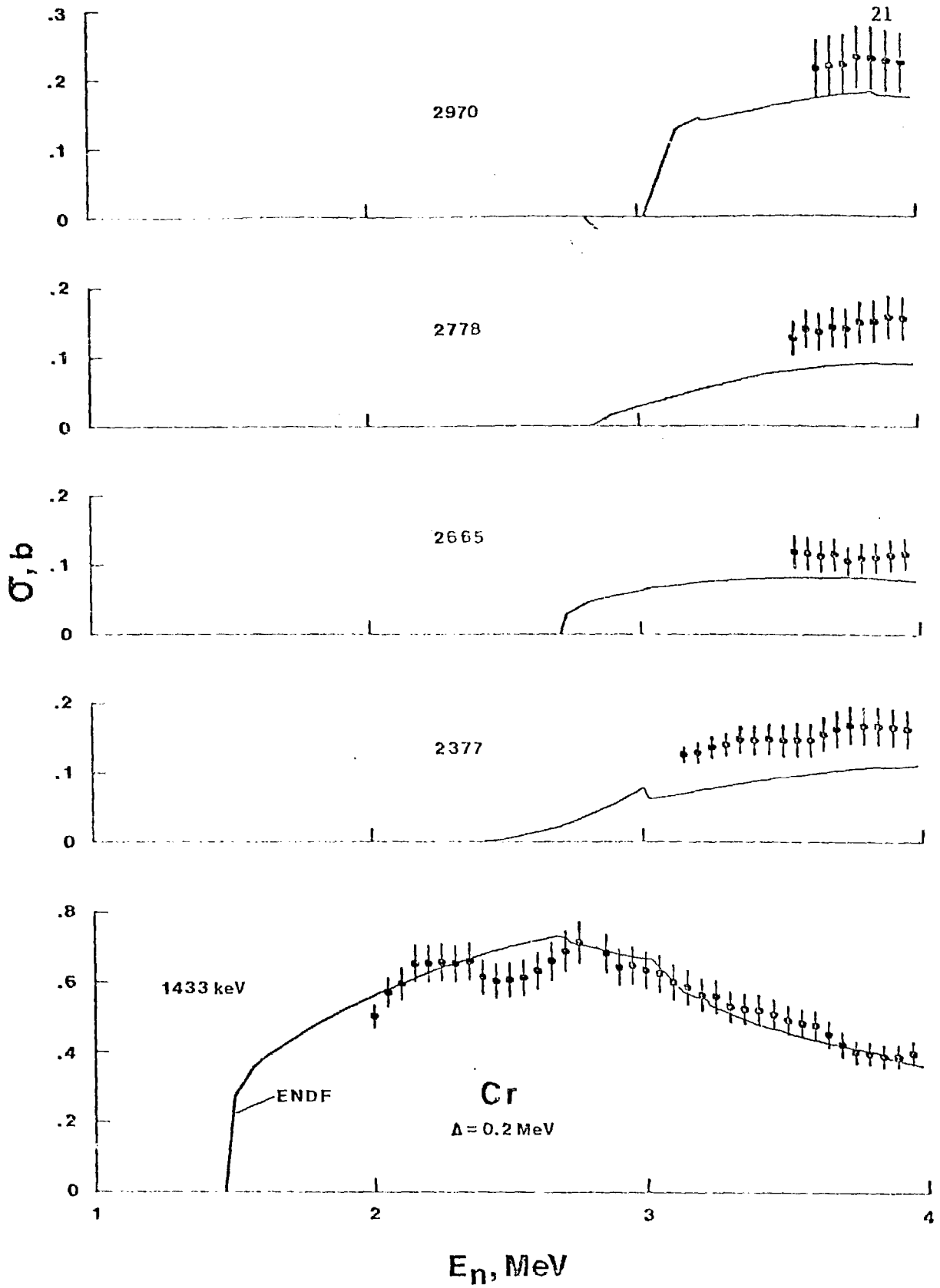

Fig. 12. Measured Inelastic Neutron Excitation Cross Sections of Elemental Chromium Averaged Over Incident Energy Intervals of 200 keV. The present measured values are indicated by solid data symbols. The curve indicates the equivalent cross sections as given in ENDF/B-IV. Observed excitation energies are numerically given in keV for each section of the figure.

levels with excitations of $\gtrsim$3.0 MeV. The resulting V (real strength) and W (imaginary strength) followed a general linear energy dependence. Superimposed on these general trends were relatively small ($\approx \pm$ 1 MeV) fluctuations with a periodicity of $\approx$0.5 MeV. These fluctuations reflected those of the underlying data bases. The fluctuations were not characteristic of a general energy-averaged behavior and were ignored in the resulting "general potentials" derived for each target. These "general potentials" were the basis for subsequent comparisons of measured and calculated values and the investigation of direct-vibrational processes. The general character of these potentials is illustrated by the ^{60}Ni example of Table IV. However, it must be stressed that these potentials are pragmatic parameterizations of the particular experimental results and are not "global" or even "regional". Indeed, there are pronounced differences as between the potentials for iron and ^{60}Ni (see Refs. 4 and 5). These differences may well be rooted in the nature of the cross section fluctuations inherent to each target. However, the "general potentials" provide an acceptable description of measured neutron-elastic-scattering cross sections of each target as illustrated in Fig. 6. Differences between measured and calculated results were generally small and random in nature as might be expected from the residual fluctuations. In addition to fluctuations, doorway levels have been reported in this lower-energy region (12). In view of these considerations the agreement of measured and calculated angle-integrated elastic scattering cross sections was judged acceptable.

Comparisons of measured and calculated neutron total cross sections follow the same general trends as those of the angle-integrated elastic-scattering cross sections. In addition to the effects of fluctuations and doorway levels there are the problems of experimental sample-size perturbations outlined above. The differences between measured and calculated values are generally within the range of estimated experimental perturbations alone. The inability of optical potentials based upon higher-energy elastic scattering to describe neutron total cross sections near 1.0 MeV in this mass region has long been observed. As outlined above, much of this discrepancy may be experimental in origin, but there may also be a shortcoming in the concept of a simple spherical optical potential. In either event, there remains an uncertainty in energy-averaged neutron total cross sections in this mass-energy region of $\approx$10% in a number of nuclides. This can be a serious concern in the context of energy-average models and in the provision of evaluated data sets for technological purposes.

The neutron-inelastic-scattering cross sections calculated using the spherical "general potentials" were qualitatively descriptive of the measured values (as illustrated in Fig. 11) but there were quantitative discrepancies. The calculated excitation of the first, 2+, levels tend to be larger than the measured values below $\approx$2.5 MeV and smaller above $\approx$3.0 MeV. These differences are $\approx$10-30%. In addition, the calculated angular distributions of scattered neutrons do not show the forward peaking observed at higher energies (see Fig. 9). Some of the comparisons between measured and calculated excitation cross sections do suggest reconsideration of some previously assigned J-Π values (see Refs. 4-5).

At higher incident energies (e.g. $\gtrsim$3.0 MeV) the above spherical interpretations have three shortocmings: a) the calculated excitations of the first,

Table IV. Spherical Optical-Potential Parameters for ^{60}Ni

Real Potential[a]		
Strength	V	$= 53.10 - 0{\cdot}3.E(MeV)$, MeV
Radius	r_V	$= 1.211$, F
Diffuseness	a_V	$= 0.614$, F
Imaginary Potential[b]		
Strength	W	$= 7.90 + 0.25{\cdot}E(MeV)$, MeV
Radius	r_W	$= 1.202$, F
Diffuseness	a_W	$= 0.596$, F

[a]Saxon form.

[b]Saxon derivative form.

*Spin-orbit terms of Thomas form and 8 MeV strength included in all calculations.

2+, levels are systematically smaller than the measured values, b) measured neutron distributions reuslting from the excitation of the first, 2+, MeV levels are not symmetric about 90 deg. as predicted by theory, and c) the measured elastic-neutron distributions deviate systematically from the calculated values as 4.0 MeV is approached. It is difficult to attribute these shortcomings entirely to fluctuations and/or the level-density approximation employed in the calculations. However, qualitatively the above features are characteristic of direct-inelastic processes. Coulomb-excitation, (γ,n) and stripping studies indicate that the first excited, 2+, levels are rotational (e.g. ^{56}Fe) or vibrational (e.g. ^{60}Ni) states. The effects of these direct interactions were estimated using a coupled-channels calculation, coupling the ground (0+) and first-excited state assuming the β_2 values of Ref. 18. In doing so it was assumed that direct and compound-nucleus processes were approximately separable and that the latter could be reasonably calculated using transmission coefficients derived from the spherical potential. The "general potentials" were used for the direct calculations except for the imaginary strengths which were adjusted to improve the description of the observed differential elastic-scattering distributions. The direct calculations were an approximation in that they did not derive transmission coefficients directly from the deformed potential nor was there an attempt made to explictly Chi-square fit the measured elastic distributions using the deformed potential. Such procedures would have been very costly and deceptive if applied to only a few measured distributions.

The coupled-channels results mitigated the shortcomings of the spherical calculations. The calculated distributions of neutrons resulting from the excitation of the first, 2+, level were peaked forward in the manner of the measured values (see Fig. 13). The inelastic cross section magnitudes and the neutron differential-scattering distributions were in much better agreement with the measured values than those obtained from the spherical calculations (as illustrated in Figs. 11 and 13). Thus the comparisons of measured and calculated values strongly suggest that direct-inelastic processes are significant in the present energy range. In particular they account for facets of the interaction not consistent with the spherical optical-statistical model. Consideration of direct-inelastic interactions does result in modifications of potential parameters relative to the spherical model (e.g. $\approx$30% reduction in imaginary strength).

V. SUMMARY REMARKS

The neutron total and scattering cross sections of chromium, iron and ^{60}Ni were measured in sufficient detail to reasonably define their energy-averaged behavior from below 1.5 MeV to above 4.0 MeV. The results are characterized by an intermediate resonance structure having periodicities and widths of several hundred keV. The energy-averaged neutron total cross sections were determined to $\approx$1% accuracies and the equivalent neutron-elastic-scattering cross sections to accuracies of $\lesssim$5%. The respective magnitudes are typically 3.5 b and 2.0 b. The implied non-elastic cross section follows to accuracies of $\approx$5%. In the present cases the non-elastic cross section is essentially equivalent to the total neutron inelastic

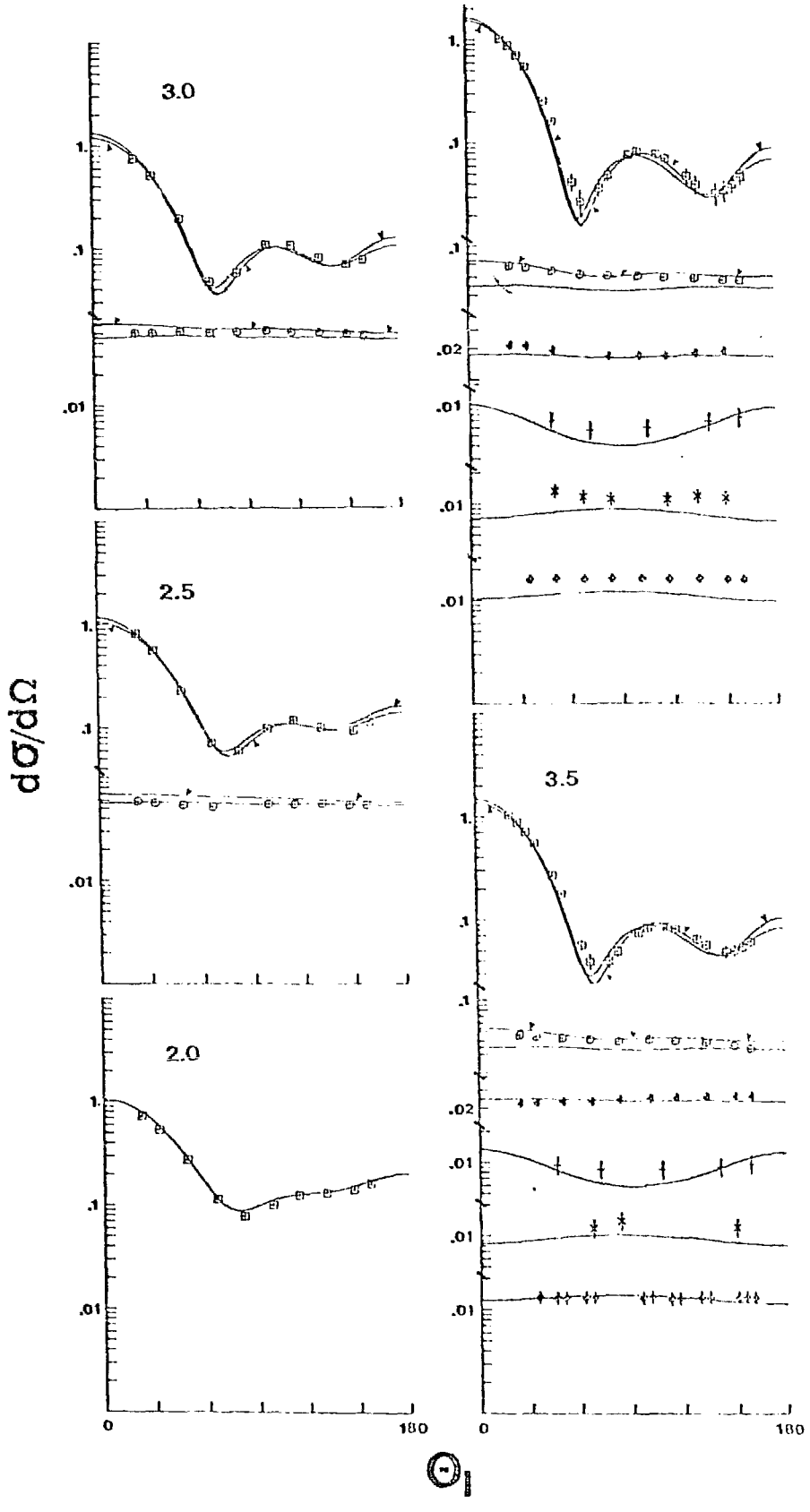

Fig. 13. Illustrative Comparisons of Measured and Calculated Differential Scattering Cross Sections of ^{60}Ni. Measured values are indicated by data points where: □ = elastic scattering, 0 = E_x of 1.342 MeV, ◁ = E_x of 2.168 MeV, + = E_x of 2.304 MeV, x = E_x of 2.509 MeV and ◇ = E_x of 2.636 MeV. Curves indicate the results of calculations, where coupled-channels results are noted with "tick" marks and spherical results with simple curves. Incident energies are given in each section of the figure in MeV. Dimensionality is cross sections in b/sr and scattering angle in lab. degrees.

scattering cross section. Thus the present neutron total and elastic-scattering measurements imply an inelastic scattering cross section satisfying a number of data requests (2) over a wide energy range. Directly measured differential inelastic-neutron scattering cross sections were consistent with the implied non-elastic cross sections to well within the respective experimental uncertainties. These experimental results suggest significant changes in the ENDF/B-IV evaluated file. Such changes do impact upon LMFBR neutronic design; for example, ≈0.15% changes in k_{eff} of a representative LMFBR system due to changes in the inelastic scattering cross section of iron alone. Optical-statistical model calculations led to results that were generally consistent with the measured values. However, strong fluctuations in this mass-energy region make explicit model fits to individual measured elastic-scattering distributions of little, if any, significance. Only comparisons over a wide energy region are meaningful. Even then it is not clear that the residual fluctuations do not continue to perturb the model choice, as the potentials derived for the various targets are different and results calculated with them have their shortcomings in comparisons with one or another aspect of the measured results. The model interpretations are further complicated by the apparent presence of direct-inelastic processes involving the excitation of vibrational or rotational levels.

REFERENCES

1. Proc. of the NEANDC/NEACRP Specialists Meeting on Nuclear Data of Structural Materials for Fast Reactors, CBNM-Geel, December, 1977, Pergamon Press, London (1979).

2. WRENDA 74, World Request List for Nuclear Data Measurements, IAEA Report, INDC(SEC)-38/U (1974).

3. A. Smith and J. Whalen, Argonne National Laboratory Report, ANL/NDM-33 (1977).

4. A. Smith, P. Guenther, D. Smith and J. Whalen, Argonne National Laboratory Report, ANL/NDM-44 (1979).

5. A. Smith and P. Guenther, Argonne National Laboratory Report, ANL/NDM-47 (1979).

6. P. Guenther, A. Smith and J. Whalen, Fast-neutron Interactions with Elemental Chromium, Argonne National Laboratory Report, to be published.

7. D. Miller, Fast Neutron Physics, Vol.-II, Eds. J. Marion and J. Fowler, Interscience Pub., New York (1963).

8. P. T. Guenther, Elastic and Inelastic Neutron Scattering from the Even Isotopes of Tungsten, Thesis, Univ. of Illinois (1977).

9. J. Hopkins and G. Breit, Nuclear Data, A9 137 (1971).

10. J. A. Harvey et al., Data available at the National Nuclear Data Center, Brookhaven National Laboratory.

11. Clement et al., Data as provided by the National Nuclear Data Center, Brookhaven National Laboratory (1971).

12. S. Cierjacks and I. Chouky, as presented at the conference of Ref. 1 (1977).

13. Nuclear Data Sheets for the various masses contributing to the present measurements.

14. H. E. Jackson, private communication (1979).

15. W. Hauser and H. Feshbach, Phys. Rev., 87 366 (1952).

16. P. A. Moldauer, Phys. Rev., 171 1164 (1963) and Phys. Rev. C11 426 (1978).

17. H. Hofmann, J. Richert, J. Tepel and H. Weidenmüller, Ann. Phys. (NY), 90 403 (1975).

18. P. Stelson and L. Grodzins, Nuclear Data, A1 21 (1965).

19. R. McKnight, private communication (1979).

20. A. Gilbert and A. G. W. Cameron, Can. Jour. Phys., 43 1446 (1965).

21. E. Barnard, J. A. M. DeVilliers, C. A. Engelbrecht, D. Reitmann and A. B. Smith, Nucl. Phys., A118 321 (1968).